# Characterization of electrical properties of AlGaN/GaN interface using coupled Schrödinger and Poisson equation

S. Das, A. K. Panda, and G. N. Dash†

National Institute of Science and Technology, Palur Hills, Berhampur, Odisha, 761008, India

**Abstract:** The electrical characterization of AlGaN/GaN interface is reported. The dependence of two-dimensional electron gas (2-DEG) density at the interface on the Al mole fraction and thickness of AlGaN layer as well as on the thickness of GaN cap layer is presented. This information can be used to design and fabricate AlGaN/GaN based MODFET (modulation doped field effect transistor) for optimum DC and RF characteristics.

**Key words:** MODFET; 2-DEG; polarization; critical thickness; self-heating

**DOI:** 10.1088/1674-4926/33/11/113001 **EEACC:** 2520

## 1. Introduction

In recent years, developments of microwave power transistors have helped to realize efficient communication systems involving a wide range of frequency of operation[1−4]. Microwave power transistors made of conventional semiconductors have already approached their performance limit. In order to meet the future needs of wireless communication systems, a great amount of effort is being put into microwave power devices like MODFET, HBT (hetero-junction bipolar transistor) etc. based on wide band gap semiconductors, among which the III-nitride based MODFETs are emerging as the potential candidate because of their exceptional power handling capability[5]. There have been considerable efforts to scale dimensions in III-nitride MODFETs to improve high-frequency performance of the transistors. At the same time efforts are being put into reducing the various non-ideal effects introduced due to device scaling. These include gate recessing to increase the device aspect ratio[6], the use of double hetero-junction structures[7], and inverted MODFET structure based on the N-polar orientation of wurtzite GaN (which exploits the reversed direction of spontaneous and piezoelectric polarization effects)[8].

In the last two decades, the AlGaN/GaN MODFETs have achieved exceptional improvements in their performance. The inherent material properties such as high breakdown field, high mobility and saturated velocity, high thermal conductivity, and wide band gap make the AlGaN/GaN MODFET a promising candidate for many microwave power applications. The combination of improved growth technology and device fabrication mechanisms have enabled devices to generate a power density up to 9.2 W/mm at 8 GHz and 30 V bias for the AlGaN/GaN MODFET with SiC as substrate. This is about ten times more than GaAs-based FETs and is thus well beyond the capability of GaAs FETs[9]. An outstanding output power performance of 40 W/mm at 4 GHz[10], a unity current gain cutoff frequency of 160 GHz[11], and a maximum frequency of oscillation of 300 GHz[12] are some noteworthy features of AlGaN/GaN MODFET performance. The cut-off frequency $f_T$ of state-of-the art AlGaN/GaN MODFETs reaches a value of 190 GHz for a gate length $L = 60$ nm[13]. With combined merits of high power and high saturation velocity[14], MODFETs made of AlGaN/GaN material combination are suitable for both electronic and optoelectronic devices. An excellent high-frequency performance, with a current gain cut-off frequency ($f_T$) of 153 GHz and power gain cut-off frequency ($f_{max}$) of 198 GHz for a gate length of 100 nm for an AlGaN/GaN MODFET using GaN/ultrathin InGaN/GaN hetero-junction as a back-barrier to the electrons in the structure have been reported[15]. The realization of high-performance 0.1-$\mu$m gate AlGaN/GaN MODFET grown on high-resistivity silicon substrates with features like cutoff frequencies as high as $f_T = 75$ GHz and $f_{max} = 125$ GHz are the highest values reported so far for AlGaN/GaN HEMTs on silicon[16]. Recent intensive research on AlGaN/GaN MODFET's has resulted in monolithic integration of two III-nitride device structures, one with enhancement-mode (E-mode) and the other with depletion-mode (D-mode) AlN/GaN/AlGaN double-heterojunction field-effect transistors (DHFETs) on a single SiC substrate through the use of etching and regrowth by molecular beam epitaxy (MBE). D-mode devices with a gate length of 150 nm had a threshold voltage $V_{th}$ of −0.10 V, a peak transconductance $g_m$ value of 640 mS/mm, and current–gain and power–gain cutoff frequencies $f_T$ and $f_{max}$ of 82 and 210 GHz, respectively. E-mode devices on the same wafer with the same dimensions had a $V_{th}$ value of +0.24 V, a peak $g_m$ value of 525 mS/mm, and $f_T$ and $f_{max}$ values of 50 and 150 GHz, respectively[17]. Also very accurate analytical models for the device are reported in Refs. [18–20]. The sheet carrier concentration and electron mobility in the channel region of an AlGaN/GaN hetero-structure grown by metal-organic vapor phase epitaxy (MOVPE) measured by Hall measurements at room temperature (300 K) and 77 K are shown in Table 1[21].

These reports have established that the AlGaN/GaN material system has excellent potential for MODFET application. It has thus opened up avenues for deeper study on this material based system for HEMT applications.

Therefore, the authors feel that a systematic study on the effect of Al mole fraction, width of AlGaN layer, thickness of GaN cap layer, etc. on the electrical properties of AlGaN/GaN interface will be very helpful to evaluate the potential of the

† Corresponding author. Email: profgndash@gmail.com
Received 14 May 2012, revised manuscript received 7 July 2012

Table 1. Mobility and sheet carrier concentration at 300 K and 77 K.

| Al mole fraction | $\mu$ (cm$^2$/(V·s)) | | $n_s$ ($10^{12}$ cm$^{-2}$) | |
|---|---|---|---|---|
| | 300 K | 77 K | 300 K | 77 K |
| 20% | 969 | 4030 | 6.2 | 5.6 |
| 27% | 1440 | 4990 | 9.8 | 10.0 |
| 35% | 1330 | 3850 | 13.0 | 15.0 |

MODFETs based on GaN material system before significant resources are dedicated to material growth, device fabrication and characterization. The basic simulation methods are described in Section 2. In Section 3, we report our results on the effect of Al concentration in the AlGaN barrier layer, thickness of AlGaN layer and thickness of GaN cap layer on 2-DEG (two-dimensional electron gas) and 2-DHG (two-dimensional hole gas) density formed at the AlGaN/GaN interface by using a simulation software developed by the authors and also verified with the results obtained by using a coupled Schrödinger–Poisson equation solver[22]. The paper is concluded in Section 4.

## 2. Methods developed for AlGaN/GaN interface properties

A novel method has been developed for the study of AlGaN/GaN interface properties and is presented in this section.

Energy band diagrams and other different results obtained for the GaN-based hetero-structures are obtained by using a computer program developed by the authors. This computer program solves self-consistently the Schrödinger's and Poisson's equations for the electron wave functions using the finite difference method (FDM) and LU-decomposition. The solution gives a detailed knowledge of electron and hole concentrations in the hetero-structures which is used to study the energy band diagrams and interfacial characteristics of hetero-structures.

The finite difference method (FDM) is a simple and efficient method for solving ordinary differential equations with simple boundary conditions. FDM can be used to solve the Schrödinger's equation. Real space is divided into discrete mesh points and the wave function is solved within those discrete spacings. The method requires the construction of mesh defining local coordinate surfaces. For each node of this mesh, the unknown wave function values are found by replacing the differential equation by difference equation. These values give the vector solution for wave function $\Psi$ and a matrix formulation of the Schrödinger equation as:

$$A\Psi = \lambda\Psi, \tag{1}$$

where $A$ is the matrix operator and $\lambda$ is the energy eigen values. Usually a uniform mesh size is selected but this method will not be effective. We need a small mesh when the wave function is changing rapidly and a large mesh during a slow change in the wave function for the ideal solution. Moreover, careful calculations are also required at the junction of two different mesh sizes and destroying the symmetry of matrix $A$, making it more difficult to calculate.

First both the Schrödinger's equation and Poisson's equation are expressed in tridiagonal matrix form using FDM technique. Then the LU-decomposition method is used to get the potential solution of the Poisson's equation. The inverse iteration method is used to solve the Schrödinger's equation to get the eigen values and corresponding eigen vectors. Then the solutions of the Schrödinger's equation and the Poisson's equation are self consistently solved to get the final potential and electron distribution.

A brief description for solving Schrödinger's equation and Poisson's equation self-consistently is given below. The one-dimensional, one electron Schrödinger equation within effective mass theory (EMA) is given as

$$-\frac{\hbar^2}{2}\frac{\mathrm{d}}{\mathrm{d}x}\left(\frac{1}{m^*(x)}\frac{\mathrm{d}}{\mathrm{d}x}\right)\Psi(x) + V(x)\Psi(x) = E\Psi(x), \tag{2}$$

where $\hbar$ is reduced Plank's constant, $m^*$ is the electron effective mass, $\Psi(x)$ is the wave function, $E$ is the eigen energy and $V(x)$ is the potential energy. Solving Eq. (2) in matrix form using FDM technique, the wave functions ($\Psi_k(x)$), corresponding eigen values ($E_k$) and Fermi energy ($E_\mathrm{f}$) is obtained.

The electron concentration for $k$th sub-band per unit area is given by

$$n_k = \int_{E_k}^{\infty} g(E)f(E)\mathrm{d}E, \tag{3}$$

where $f(E)$ is the Fermi–Dirac distribution function given by

$$f(E) = \frac{1}{1+\exp[(E-E_\mathrm{f})/KT]}, \tag{4}$$

and $g(E)$ is the 2-D density of states for a single sub-band in a quantum well system given by

$$g(E) = \frac{m^*}{\pi\hbar^2}. \tag{5}$$

Using Eqs. (3), (4) and (5), we get

$$n_k = \frac{m^*}{\pi\hbar^2}\int_{E_k}^{\infty}\frac{1}{1+\exp(E-E_\mathrm{f})/KT}, \tag{6}$$

where $K$ is the Boltzmann constant and $T$ is temperature in Kelvin.

The wave function $\Psi_k(x)$ is related to the electron density per unit area $n'(x)$ inside the structure given by

$$n'(x) = \sum_{k=1}^{m}\Psi_k^*(x)\Psi_k(x)n_k, \tag{7}$$

$$n'(x) = \sum_{i=1}^{m}\frac{m^*K_T}{\pi\hbar^2}\ln[1+\exp(E_\mathrm{f}-E_k)/KT]|\Psi_k(x)|^2, \tag{8}$$

where $m$ is the number of bound states, $\Psi_k(x)$ is the position dependent wave function and $\Psi_k^*(x)$ is the complex conjugate of $\Psi_k(x)$.

The $n'(x)$ distribution obtained above after being expressed in per unit volume as $n(x)$ is now being put in the 1-D Poisson equation given by

$$\frac{\mathrm{d}}{\mathrm{d}x}\left(\varepsilon_\mathrm{s}(x)\frac{\mathrm{d}}{\mathrm{d}x}\right)\phi(x) = \frac{-q\,[N_\mathrm{D}(x)-n(x)]}{\varepsilon_\mathrm{o}}, \tag{9}$$

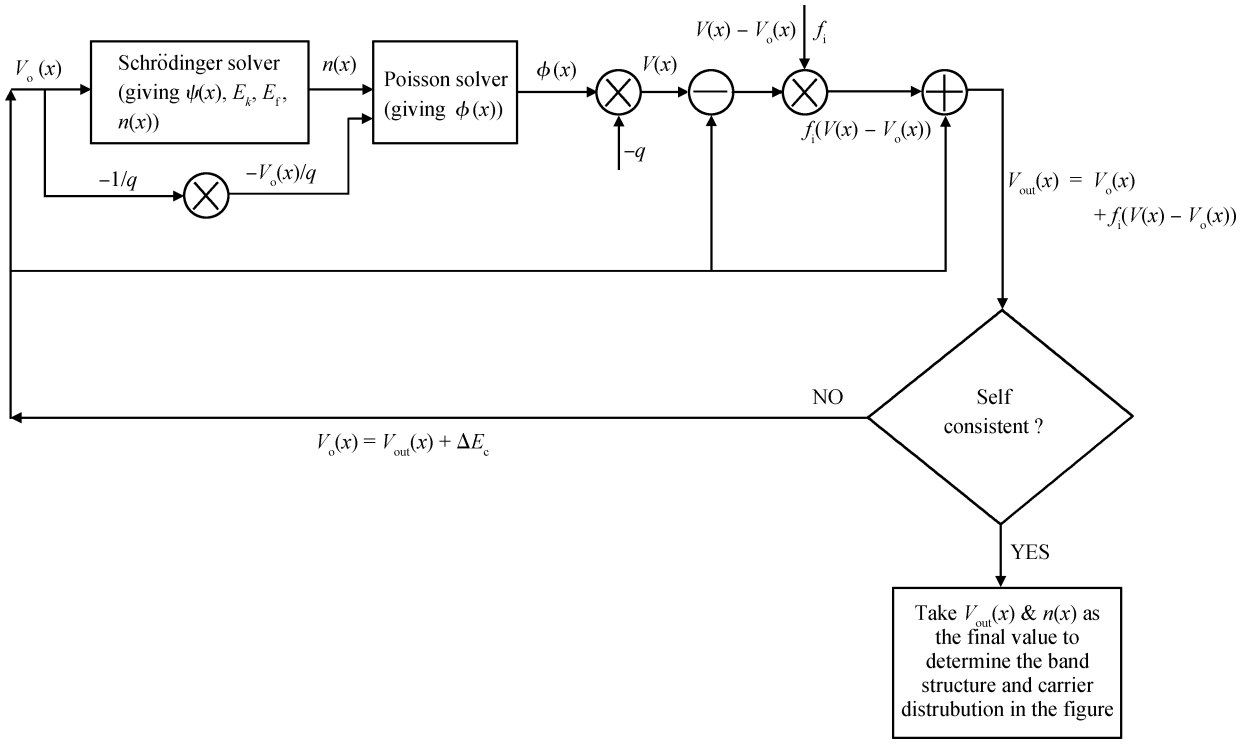


Fig. 1. Iteration process showing the self-consistent solution of Schrödinger wave equation and Poisson equation.

where $\varepsilon_s(x)$ is the position dependent dielectric constant, $\phi(x)$ is the electrostatic potential and $N_D(x)$ is the ionized donor concentration and $n(x)$ is the electron density distribution per unit volume. Solving Eq. (3) in matrix form again using FDM technique, an electrostatic potential $\phi(x)$ is obtained.

This $\phi(x)$ is used to calculate the updated new potential energy distribution as

$$V_{out}(x) = f_i[-q\phi(x) + V_0(x)] + V_0(x) + \Delta E_c, \qquad (10)$$

where $\Delta E_c$ is the pseudo potential energy due to the conduction band offset at the hetero-junction, $V_0(x)$ is the potential energy distribution used in the present iteration and $f_i$ is the scaling factor ranging from 0.05 to 0.1.

For AlGaN/GaN material, the total polarization charge at the interface must be taken into account in the Poisson equation for calculations of the sheet carrier concentration as $E_{AlGaN}\varepsilon_{AlGaN} - E_{GaN}\varepsilon_{GaN} = -\sigma$ where $E$ is the electric field, $\varepsilon$ is the dielectric constant and $\sigma$ is the polarization charge density at the interface.

The total polarization charge can also be written as $P_{TOTAL} = P_{PZ} + P_{SP}$, where $P_{PZ}$ is the piezoelectric charge caused by the lattice mismatch and by the thermal strain given by $P_{PZ} = P_{MIS} + P_{TS}$ where $P_{MIS}$ is the piezoelectric charge due to lattice mismatch and $P_{TS}$ is the piezoelectric charge due to thermal strain, whereas $P_{SP}$ represents the spontaneous polarizability of the GaN/AlGaN interface, as clearly demonstrated by the works of Bernardini *et al.*[23]. Actually the piezoelectric and spontaneous polarization charge is inextricable from the gate-induced and charge induced by doping in barrier layer and so it must be carefully considered in device design and analysis.

These are the basic equations required to be solved for finding the solution to the Schrödinger's equation and Poisson's equations self-consistently.

The procedure of our algorithm is then divided into the following steps:

(1) We start with a trial potential energy value of $V_0(x)$ and then calculate the wave functions $\Psi(x)$ and the corresponding eigen energies $E_k$ using matrix representation of Schrödinger's wave equation (2) using FDM method.

(2) Then the values associated with $n_k$ are found out using Eq. (6).

(3) Then the electron density distribution $n'(x)$ is calculated by using the equations given for $n'(x)$ above as Eq. (8).

(4) The above calculated value of $n'(x)$ is then expressed in per unit volume $n(x)$ and along with the given donor concentration $N_D(x)$ and total polarization charge $P_{TOTAL}$, 1-D Poisson's equation (9) is solved to obtain $\phi(x)$ and from this a new potential energy $V(x)$ is obtained using Eq. (10).

(5) Again we use this new value of $V(x)$ in the Schrödinger's equation to find new values of wave function $\Psi(x)$ and the corresponding eigen energies $E_k$.

In this way, the iterations will continue till it yields self-consistent solutions for $V(x)$ and $n(x)$ i.e. the iteration is repeated until convergence is achieved. After getting the self-consistent solutions for $V(x)$ and $n(x)$, these values of $V(x)$ and $n(x)$ can be used to determine the band diagram as well as carrier concentration in the channel. The iteration procedure used in the program is shown in Fig. 1.

## 3. Results and discussion

In this section, we explain the simulation results and also examine the different parameters' variation effects.

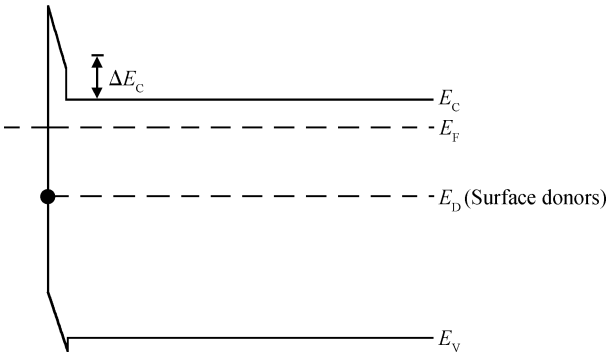


Fig. 2. Simulated energy band diagram of AlGaN ($x = 0.30$)/GaN heterostructure with AlGaN layer thickness = 2.5 nm.

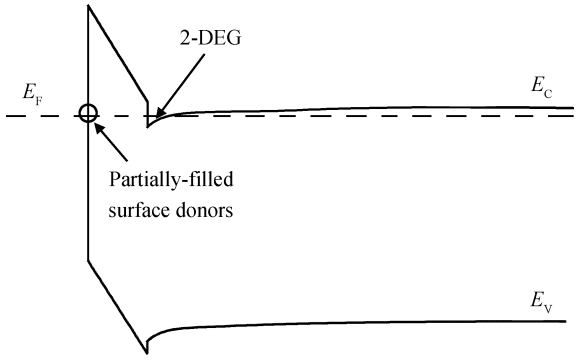


Fig. 4. Energy band diagram illustrating the surface donor model with undoped $Al_{0.3}Ga_{0.7}N$ with barrier thickness greater than the critical thickness for the formation of 2-DEG.

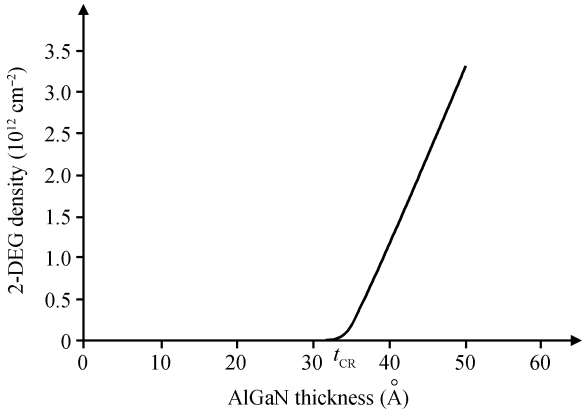


Fig. 3. Simulated values for $Al_{0.3}Ga_{0.7}N$ thickness versus 2-DEG density.

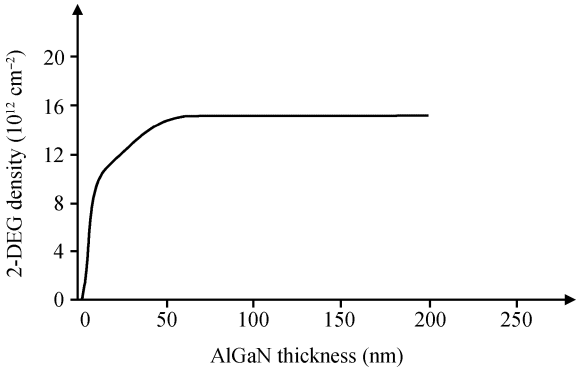


Fig. 5. Simulated values for $Al_{0.3}Ga_{0.7}N$ thickness versus 2-DEG density.

### 3.1. Effect of AlGaN layer thickness on the energy band diagram and the sheet carrier density

We have considered a single AlGaN/GaN hetero-structure with 30% Al composition and undoped GaN and AlGaN layers. The thickness of the AlGaN layer is varied starting from a very low value of 10 Å to a value of 35 Å while the thickness of the buffer layer is made constant at 50 nm. This structure is simulated using the author's developed program. The simulated energy band diagram for AlGaN layer thickness of 25 Å is shown in Fig. 2. In the above structure since the surface states are lying below $E_F$ (Fermi energy level) as shown in Fig. 2 and the energy level lying below Fermi energy level is considered to be filled, so these surface states are neutral. Since the surface state is sufficiently deep because it lies below $E_F$, there will be no formation of 2-DEG and so for all practical purposes 2-DEG density will be zero.

Figure 3 shows the variation of 2-DEG density as a function of thickness of $Al_{0.3}Ga_{0.7}N$ layer. As we can see from Fig. 3, the 2-DEG density starts increasing rapidly after a certain thickness of the AlGaN layer. This thickness is called the critical thickness $t_{CR}$ (here the critical thickness is found to be around 35 Å). The critical thickness depends on factors such as the alloy composition and the doping concentration of the layers. Figure 4 shows the simulated band diagram of the structure when the thickness of the $Al_{0.3}Ga_{0.7}N$ layer is greater than the critical thickness. The 2-DEG formation is clearly shown in this figure.

Figure 5 shows the graph between the thicknesses of $Al_{0.3}Ga_{0.7}N$ layer and the 2-DEG density for thickness ranging from 2.5 to 200 nm. As the thickness of the $Al_{0.3}Ga_{0.7}N$ layer is increased, the 2-DEG density also increases and saturates after a certain value. It can be seen from Fig. 5 that as the $Al_{0.3}Ga_{0.7}N$ barrier thickness is increased, the sheet density also increases but it reaches the value of the polarization induced charge after a certain value of the thickness. This is the maximum value of the sheet concentration that can be obtained for that particular composition (i.e. $x = 0.3$).

### 3.2. Effect of Al mole fraction in AlGaN/GaN structures

For a single hetero-structure of AlGaN/GaN, with the thickness for both GaN and AlGaN layers fixed, the effect of Al mole fraction on the 2-DEG layer density is simulated. The simulated band diagram for the hetero-structure with the thickness of $Al_xGa_{1-x}N$ layer as 5 nm and GaN layer thickness of 50 nm is shown in Fig. 6 for $x = 0.05$.

As can be seen from the figure, the 2-DEG formation is not as pronounced for a low value of alloy composition. For this very small value of $x = 0.05$ (i.e. for 0.05% of Al), the value of the sheet carrier density in the above structure is found out to be $8.51 \times 10^{12}$ cm$^{-2}$. This density value is smaller than the value obtained for an alloy composition used in practical purposes of $x = 0.3$ to 0.4. The dependence of sheet carrier density on the alloy composition value $x$ is shown in Fig. 7 which shows that

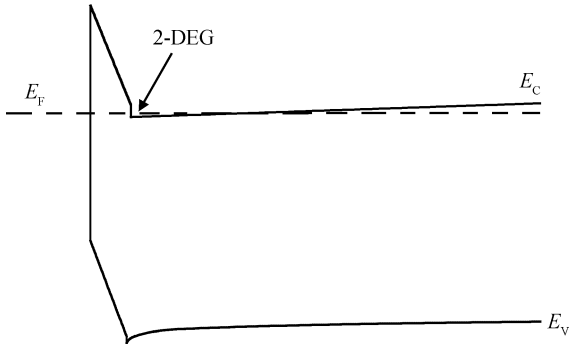


Fig. 6. Simulated band diagram of $Al_{0.05}Ga_{0.95}N$/GaN heterostructure for $x = 0.05$.

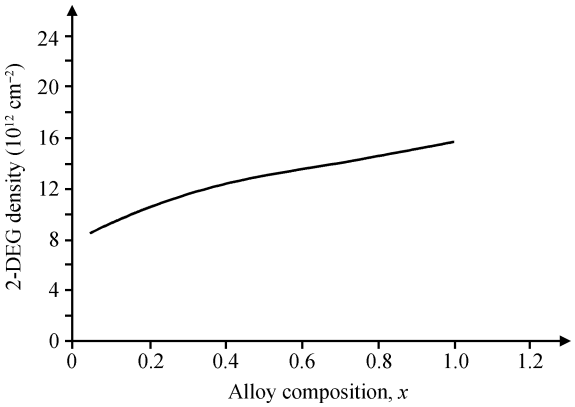


Fig. 7. Sheet carrier density in AlGaN/GaN structure as a function of AlGaN barrier composition $x$.

as the value of alloy composition is increased, the sheet density also increases and almost has a linear relationship between the two. This can be explained in the following way.

From literature available, the spontaneous polarization and piezoelectric polarization charge per unit area in GaN[24] are given by $P_{\text{sp, GaN}} = -0.029$ C/m$^2$ and $P_{\text{pz, GaN}} = 0.0163x$ C/m$^2$, respectively where $x$ is the aluminum mole fraction in AlGaN grown on GaN substrate pseudomorphically.

The spontaneous polarization charge of AlGaN is obtained from the linear interpolation of the values in GaN (–0.029 C/m$^2$) and AlN (–0.081 C/m$^2$) and is given as[25]

$$P_{\text{sp, AlGaN}} = (-0.052x - 0.029)\ \text{C/m}^2.$$

The piezoelectric polarization charge for AlGaN[25] is written as

$$P_{\text{pz, AlGaN}} = 2\varepsilon_1 \left[ e_{31} - e_{33} \left( \frac{C_{13}}{C_{33}} \right) \right] \text{C/m}^2,$$

where $C_{ij}$ are the elastic tensor components[24], $e_{ij}$ the piezoelectric tensors[24] and $\varepsilon_1$ is the isotropic in-plane strain[24] which is given by $\varepsilon_1 = \frac{a - a_0)}{a_0}$ , where $a_0$ is the lattice constant of relaxed GaN over which AlGaN is grown and $a(x) = -0.077x + 3.189$ Å is the lattice constant of $Al_xGa_{1-x}N$. It is thus clear that the piezoelectric charge in AlGaN is a linear function of $x$.

Finally, AlGaN/GaN hetero-interface charge density in per unit area is given by

$$\sigma = \Delta P = P_{\text{AlGaN}} - P_{\text{GaN}}$$
$$= \left(P_{\text{SP}}^{\text{AlGaN}} + P_{\text{PZ}}^{\text{AlGaN}}\right) - \left(P_{\text{SP}}^{\text{GaN}} + P_{\text{PZ}}^{\text{GaN}}\right)\ \text{C/m}^2,$$

where $P_{\text{AlGaN}}$ is the total polarization charge in the AlGaN layer and $P_{\text{GaN}}$ is the total polarization charge in the GaN layer.

The electron sheet concentration for this polarization charge density can be calculated as

$$n_s = \frac{\sigma}{e}\ \text{m}^{-2}.$$

From the above discussion we observed that $\sigma$ is a linear function of Al mole fraction and hence $n_s$, which explains the nearly linear relationship of $n_s$ with $x$ obtained from our simulation.

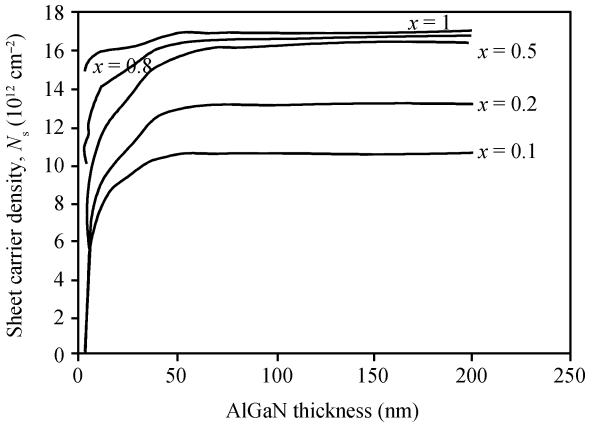


Fig. 8. Sheet carrier density dependence on the AlGaN barrier thickness for various values of the alloy composition.

### 3.3. Sheet carrier density dependence on the AlGaN barrier thickness for various values of the alloy composition

Figure 8 shows the simulated results for the dependence of the carrier sheet density on the AlGaN layer thickness for various values of alloy composition ranging from $x = 0.1$ to $x = 1$ (pure AlN). From the graph it is clear that the sheet carrier density increases with both the thickness of the barrier and the alloy composition value, $x$. For all values of $x$, the sheet density starts saturating at a thickness little over 50 nm. For small values of $x$, sheet carrier density increases right after critical thickness and saturates with a value near the value of the polarization induced charge.

So as $x$ increases, the dependence of the sheet density on the barrier thickness is not as rapid as in the case of low values of $x$. As $x$ approaches 1, that is when AlGaN is almost an AlN layer; the dependence on the thickness is almost negligible after a certain thickness. Also the sheet carrier density for 200 nm AlGaN barrier when $x = 0.8$ and when $x = 1$ are almost the same as $1.7 \times 10^{13}$ cm$^{-2}$. Hence this value is the maximum sheet carrier density that is obtained from the simulations of the AlGaN/GaN hetero-structure.

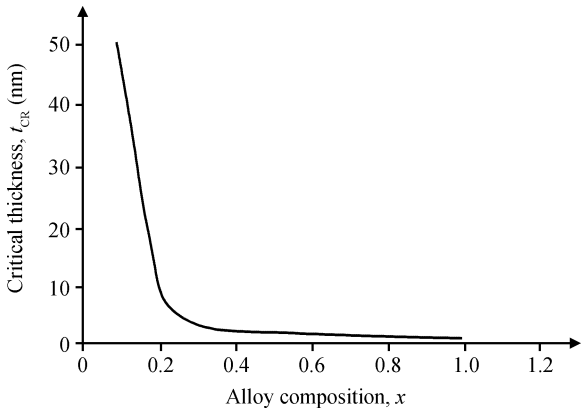


Fig. 9. Critical thicknesses as a function of Alloy composition in AlGaN.

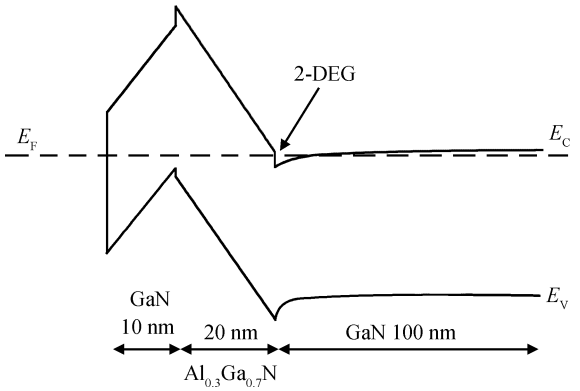


Fig. 10. Simulated band diagram of GaN/AlGaN/GaN heterostructure for 10 nm thickness of GaN cap layer.

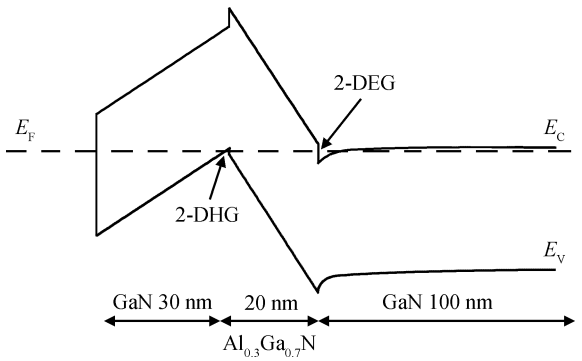


Fig. 11. Simulated band diagram of GaN/AlGaN/GaN heterostructure for 15 nm thickness of GaN cap layer.

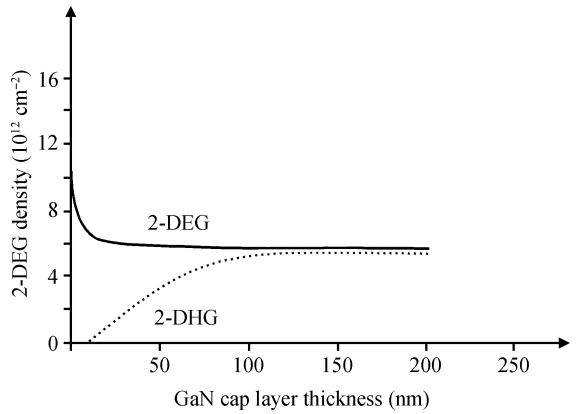


Fig. 12. Dependence of the sheet density on GaN cap layer thickness. Solid line represents 2-DEG sheet density and the dotted line represents 2-DHG density.

### 3.4. Critical thickness dependence on alloy composition

The simulated result for the dependence of the critical thickness on the alloy composition is shown in Fig. 9. The critical thickness, for a very low value of $x$ is very high but it decreases rapidly as the alloy composition is increased. After a certain point it decreases slowly and has the minimum critical thickness of 0.5 nm for an AlN/GaN structure.

Critical thickness depends upon the relative difference of the lattice constant of the two layers and the lattice constant of the AlGaN layer depends upon its Al mole fraction. The AlGaN layer, whose lattice constant is different from that of the substrate, can be grown till the critical thickness of the layer is reached, so that it still has the single crystal structure without any physical defects or dislocations (i.e. incomplete bonds at the interface). But it should be noted that the grown layer is a strained layer referred to as pseudomorphic layer. The strained layer can sometimes give the peculiar property of higher mobility in comparison to the unstrained layer. But if we keep on growing the epitaxial layer beyond its critical thickness which in turn depends upon the Al mole fraction, then the strained layer will get pulled back to its original lattice structure which is its minimum energy position and there will be discontinuity in the lattice structure at the interface. The defects will be created at the interface because of this discontinuity at the interface. This in turn will reduce the mobility of carriers and hence device performance.

### 3.5. Formation of 2-DHG (two-dimensional hole gas)

Simulation is performed by introducing a GaN cap layer on the top of the AlGaN/GaN hetero-structure. Here the undoped AlGaN has an alloy composition of $x = 0.30$ and a thickness greater than the critical thickness (note that for this particular hetero-structure the critical thickness is found to be around 15 nm). Simulations have been carried out for different values of thickness of the GaN cap layer. When the GaN layer thickness is very small (say 10 nm), the simulated energy band diagram shown in Fig. 10 is obtained which shows formation of 2-DEG. As the GaN cap layer thickness is increased to 30 nm, a 2-DHG is also formed but at the same time the 2-DEG density decreases as shown in Fig. 11.

This phenomenon is explained as follows. When a GaN cap layer is added to the AlGaN/GaN hetero-structure, a negative polarization charge is introduced at the interface between the GaN cap layer and the AlGaN layer. This causes a decrease in the 2-DEG density and an increase in the electric field in the AlGaN layer. As the thickness of the cap layer is increased, the valence band at the upper interface shifts upwards reaching the Fermi level after a certain thickness. At this point, a 2-DHG is formed at the upper interface and this stops any increase of the electric field in the AlGaN layer.

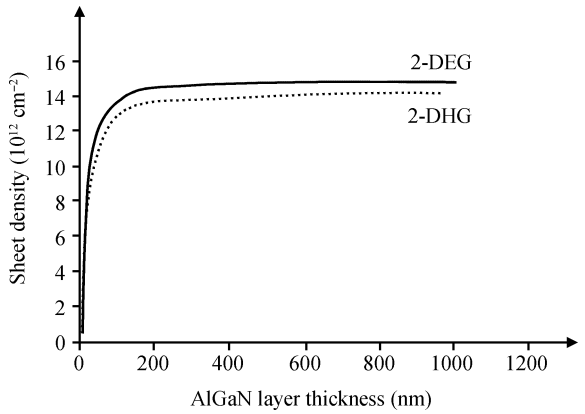


Fig. 13. Sheet density dependence on the AlGaN barrier thickness. Solid line represents 2-DEG sheet density and the dotted line represents 2-DHG density.

### 3.6. Effect of GaN cap layer thickness on the sheet density

The dependence of the 2-DEG and the 2-DHG sheet densities for various GaN layer thicknesses are shown in Fig. 12. When there is no cap layer, the 2-DEG density is at its maximum. The introduction of the cap layer decreases this density and as the thickness of the cap layer increases the 2DEG density decreases rapidly until a 2DHG is formed.

For this particular structure this thickness was found to be 15 nm. After this point the 2-DEG decreases slowly and becomes constant after some point. The dotted line represents the 2-DHG density in the upper interface in the structure. It remains zero till the valence band reaches the Fermi level and the 2-DHG starts to form after 15 nm of cap layer thickness. After this, the 2-DHG starts increasing as the cap layer thickness is increased and the density saturates as the thickness is further increased.

### 3.7. Thick GaN-capped GaN/AlGaN/GaN structures

The GaN cap layer is chosen to be thick enough so that both the densities are saturated and the effect of varying the AlGaN barrier thickness is studied. The hetero-structure used for the simulation has a GaN buffer layer thickness of 50 nm and $x = 0.3$ with varying barrier layer thickness. The dependence of the sheet densities on the thickness of the AlGaN layer in the presence of a thick GaN cap layer is shown in Fig. 13. As the thickness is increased the densities are also increased, rapidly at first and then it saturates after a certain thickness because, since a thick cap is used, the surface effects are removed from the two-dimensional carrier gases.

## 4. Conclusion

In this paper, a systematic approach regarding the properties of the AlGaN/GaN interface has been extensively studied for high speed device applications. This allows a better understanding of the ways to achieve higher performance levels for GaN based high speed devices like MODFET. A critical thickness of 35 nm for the AlGaN layer at an alloy composition of 0.3 for the formation of 2-DEG is noteworthy. Similarly a minimum cap layer of 15 nm is required for the formation of 2-DHG. The sheet carrier concentration increases almost linearly with the increase of the Al mole fraction. This result is consistent with the Hall measurements of Lu *et al.*[21]. We believe that these data will be of great help to the manufacturer of high speed GaN based devices.

## References

[1] Harvard E, Brown R, Shealy J R. Performance of AlGaN/GaN high-electron mobility transistors with AlSiN passivation. IEEE Trans Electron Devices, 2011, 58(1): 87

[2] Heller E R, Vetury R, Green D S. Development of a versatile physics-based finite-element model of an AlGaN/GaN HEMT capable of accommodating process and epitaxy variations and calibrated using multiple DC parameters. IEEE Trans Electron Devices, 2011, 58(4): 1091

[3] Higashiwaki M, Pei Y, Chu R, et al. Effects of barrier thinning on small-signal and 30-GHz power characteristics of AlGaN/GaN heterostructure field-effect transistors. IEEE Trans Electron Devices, 2011, 58(6): 1681

[4] Chiou Y L, Lee C T. Band Alignment and performance improvement mechanisms of chlorine-treated ZnO-gate AlGaN/GaN metal–oxide–semiconductor high electron mobility transistors. IEEE Trans Electron Devices, 2011, 58(11): 3869

[5] Eastman L F, Mishra U K. The toughest transistor yet. IEEE Spectr, 2002, 39(5): 28

[6] Kuliev A. 0.15 $\mu$m gate-length AlGaN/GaN HEMTs with varying gate recess length. Solid-State Electron, 2003, 47(1): 117

[7] Micovic M, Hashimoto P, Hu M, et al. GaN double heterojunction field effect transistor for microwave and millimeter wave power applications. IEDM Tech Dig, 2004: 807

[8] Rajan S, Chini A, Wong M H, et al. N-polar GaN/AlGaN/GaN high electron mobility transistors. J Appl Phys, 2007, 102(4): 044 501

[9] Sheppard S T, Doverspike K, Pribble W L, et al. High-power microwave GaN/AlGaN HEMT's on semi-insulating silicon carbide substrates. IEEE Electron Device Lett, 1999, 20: 161

[10] Wu Y, Moore M, Saxler A, et al. 40-W/mm double field-plated GaN HEMTs. Proc 64th Device Res Conf, 2006: 151

[11] Kim D, Kumar V, Lee J, et al. Recessed 70-nm gate-length AlGaN/GaN HEMTs fabricated using an $Al_2O_3/SiN_x$ dielectric layer. IEEE Electron Device Lett, 2009, 30(9): 913

[12] Chung J W, Hoke W E, Chumbes E M, et al. AlGaN/GaN HEMT with 300-GHz $f_{max}$. IEEE Electron Device Lett, 2010, 31(3): 195

[13] Higashiwaki M, Mimura T, Matsui T. AlGaN/GaN heterostructure field-effect transistors on 4H-SiC substrates with current-gain cutoff frequency of 190 GHz. Appl Phys Express, 2008, 1(2): 021103

[14] Oxley C H, Uren M J, Coates A, et al. On the temperature and carrier density dependence of electron saturation velocity in an AlGaN/GaN HEMT. IEEE Trans Electron Devices, 2006, 53(3): 565

[15] Palacios T, Chakraborty A, Heikman S, et al. AlGaN/GaN high electron mobility transistor with InGaN back-barriers. IEEE Electron Device Lett, 2006, 27(1): 13

[16] Sun H, Alt A R, Benedickter H, et al. High performance 0.1-$\mu$m gate AlGaN/GaN HEMTs on silicon with low-noise figure at 20 GHz. IEEE Electron Device Lett, 2009, 30(2): 107

[17] Brown D F, Shinohara K, Williams A, et al. Monolithic integration of enhancement and depletion-mode AlN/GaN/AlGaN DHFETs by selective MBE regrowth. IEEE Trans Electron Devices, 2011, 58(4): 1063

[18] Cheng X, Wang Y. A surface-potential-based compact model for AlGaN/GaN MODFETs. IEEE Trans Electron Devices, 2011, 58(2): 448

[19] Esposto M, Chini A, Rajan S. Analytical model for power switching GaN-based HEMT design. IEEE Trans Electron Devices, 2011, 58(5): 1456
[20] Mudanai S, Roy A, Kotlyar R, et al. Capacitance compact model for ultrathin low-electron-effective-mass materials. IEEE Trans Electron Devices, 2011, 58(12): 4204
[21] Lu W, Kumar V, Piner E L, et al. DC, RF, and microwave noise performance of AlGaN–GaN field effect transistors dependence of aluminum concentration. IEEE Trans Electron Devices, 2003, 50(4): 1069
[22] Tan I H, Snider G L, Hu E L. A self-consistent solution of Schrödinger–Poisson equations using a nonuniform mesh. J Appl Phys, 1990, 68(8): 4071
[23] Bernardini F, Fiorentini V, Vanderbilt D. Spontaneous polarization and piezoelectric constants of III–V nitrides. Phys Rev B, 1997, 56: R10024
[24] Ambacher O. Review article-growth and applications of group III-nitrides. J Phys D: Appl Phys, 1998, 31: 2653
[25] Ambacher O, Smart J, Shealy J R, et al. Two-dimensional electron gases induced by spontaneous and piezoelectric polarization charges in N- and Ga-face AlGaN/GaN heterostructures. J Appl Phys, 1999, 85(6): 3222